# Modeling of mass transfer in combination with a homogeneously catalyzed reaction

Hoorn, J.A.A.; Versteeg, G. F.

*Published in:*
AIChE Journal

*DOI:*
10.1002/aic.10869

ELSEVIER

Chemical Engineering Science 61 (2006) 5137–5148

Chemical Engineering Science

www.elsevier.com/locate/ces

# Modelling of mass transfer in combination with radical reactions

J.A.A. Hoorn[a,*], G.F. Versteeg[b]

[a]DSM Research, P.O. Box 18, 6160 MD Geleen, Netherlands
[b]Department of Chemical Engineering, University of Twente, P.O. Box 217, 7500 AE Enschede, Netherlands

Received 27 July 2005; received in revised form 3 February 2006; accepted 6 March 2006
Available online 20 March 2006

**Abstract**

The diffusion–reaction equations for different model versions have been solved using a finite-differencing technique. In all models a reactant A is transferred from the gas to the liquid phase and reacts in the liquid with B to form P. The calculations comprised a simple stoichiometric model, a system with radical intermediates involved in the propagation steps and a version where also the termination reactions were included. The results show that the diffusion coefficients of radical intermediates can have significant influence on the profiles of concentrations and reaction rates near the G/L interface. Furthermore, it is shown that for very fast reactions differences in diffusion coefficients of the intermediates influence the by-product formation. For systems of two radical intermediates, the so-called mixed termination product is only formed in low quantities whereas the other two termination products dominate. The calculation of enhancement factors required in the design of a G/L reaction system can be performed with simplified models where the reactive intermediates do not occur in the expressions for the reaction rates. The optimum model for a specific design purpose can be found by tuning the functions that correlate the parameters of the complex model to the parameters of the simplified model. In principle it is possible to very easily evaluate a large number of alternatives.


*Keywords:* Absorption; Design; Diffusion; Mass transfer; Modelling; Model reduction

## 1. Introduction

The calculation of the rate of mass transfer in the absorption of gases followed by complex chemical reaction is a challenging task. The textbook example of a single first-order irreversible reaction is often a drastic simplification of real reaction systems. However, the concepts of Hatta number and enhancement factor are simple and well established. A great number of researchers have investigated a wide variety of chemical reaction systems in which one or more reactants or product species absorbs or desorbs. The spectrum of reactive systems includes single and multiple reactions (parallel and in-series), irreversible as well as reversible reactions and auto catalytic reactions. A comprehensive overview on the literature on mass transfer accompanied by complex chemical reactions can be found in Van Swaaij and Versteeg (1992). In industry, reactions involving radical intermediates are frequently encountered. Examples are oxidation and chlorination reactions. In the fine chemical industry, gas/liquid processes such as bromination or ozonolysis proceed through radical intermediates. Already the simplest reaction mechanisms involving radical intermediates comprise multiple reaction schemes. Only in the case of a specific definition, a single irreversible reaction, analytic solutions to the diffusion–reaction equations can be found. One example of such a special case is given by Sim and Mann (1975). They studied the autocatalytic reaction:

$$A + R\bullet \rightarrow R\bullet + R\bullet. \quad (1)$$

The authors applied the film theory to calculate the rate of absorption and the enhancement factors. The equations were solved through a numerical procedure involving integration of a system of first order differential equations by a modified Runge–Kutta method (Juvekar, 1976, suggested an improved solution technique). In addition, Flores-Fernandez and Mann (1978) published a paper with a comparison between film and penetration models for the aforementioned reaction. Another example, not directly in the field of chemical reactors, was presented by Burns et al. (1970). The radiolysis of cyclohexane

* Corresponding author. Tel.: +31 46 4761147; fax: +31 46 4760809.
*E-mail address:* johan.hoorn@dsm.com (J.A.A. Hoorn).

0009-2509/$ - see front matter © 2006 Elsevier Ltd. All rights reserved.
doi:10.1016/j.ces.2006.03.007

was described with the following set of reactions:

$$C_6H_{12} \longrightarrow C_6H_{12}^{**} \rightarrow H_2 + C_6H_{10},$$
$$C_6H_{12} \longrightarrow C_6H_{12}^{*} \rightarrow H\bullet + C_6H_{11}\bullet. \quad (2)$$

A point source of radicals was created by the radiation energy in the liquid. In the models the point sources were approximated by Gaussian spherical or cylindrical distributions. Burns et al. (1970) included a number of propagation and termination reactions in their models.

Reactions involving radical intermediates are in general fast to very fast reactions. For radicals, the reaction rate constants are typically in the range of $10^5$–$10^9$ $m^3$/kmol/s for second order reactions (Carey and Sundberg, 1990; Sitarski, 1981). For very fast or instantaneous reactions the equations of Higbie's penetration theory can be solved analytically.

For a single irreversible instantaneous reaction of the type A + B → P the enhancement factor and the location of the reaction plane can be found from an implicit equation that has to be solved for a parameter $\beta$ (definitions according to Froment and Bischoff, 1990):

$$\exp\left(\frac{\beta^2}{D_B}\right)\operatorname{erfc}\left(\frac{\beta}{\sqrt{D_B}}\right) = \frac{a}{b}\frac{c_{B,0}}{c_{A,i}}\cdot\sqrt{\frac{D_B}{D_A}}\exp\left(\frac{\beta^2}{D_A}\right) \times \operatorname{erf}\left(\frac{\beta}{\sqrt{D_A}}\right). \quad (3)$$

The constants $a$ and $b$ are the stoichiometric coefficients for the reactants A and B, respectively. For any time $t$ the position of the reaction front ($\delta_r$) is given by

$$\delta_r = 2\cdot\beta\cdot\sqrt{t}. \quad (4)$$

The enhancement factor (for an infinitely fast reaction) is given by

$$E_{A,\infty} = \frac{1}{\operatorname{erf}(\beta/\sqrt{D_A})}. \quad (5)$$

## 2. Model systems studied

Three model systems have been considered, all concerned with A as a gaseous component from the gas phase transferring to the liquid and reacting with B to form product P. The reaction pathways make the difference. The models have been given short names to reflect their essential feature.

### 2.1. Model ABP

This is the model for the stoichiometric reaction:

$$A + B \rightarrow P. \quad (6)$$

### 2.2. Model 3T

This model is based on a small network of reactions involving radical intermediates. The system comprises six reactions as shown in Fig. 1. The source of radicals originates from a suitable initiator (In•) that reacts with B to generate the radical equivalent of B. The propagation steps are formed by two reactions: B• reacts with A to form P•, reaction of this radical with B gives P and B• . Three by-products from termination reactions can be formed. The number of parameters in model 3T is already quite large. Besides reaction rate constants also diffusion coefficients, volatility for each component and mass transfer parameters can be varied.

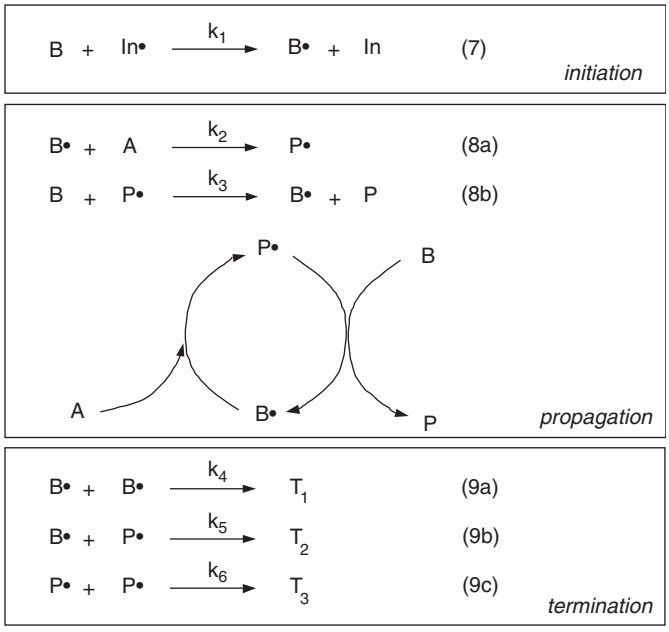


Fig. 1. Components and reactions in the model 3T.

### 2.3. Model BPdot

This third model is a simplified version of model 3T comprising only the two propagation reactions, Eqs. (8a) and (8b), respectively. The initiation reaction, Eq. (7), has been left out because it is assumed that the reaction is so fast that all radicals are in the form of B• at the start. The termination reactions can be omitted because the termination products do not interfere with the propagation steps. This simplified model has been included in the analysis because part of the effects can be studied more effectively in a system with fewer parameters.

For all model systems assumptions have been made:

- diffusion is described by Fick's laws; there are no convective contributions in the liquid phase to mass transport,
- the solvent is inert,
- the temperature is constant, heat effects of reactions and absorption are not included,
- the density of the liquid is constant,
- mass transfer resistance in the gas phase can be included in the model calculations, but the study of its effects is included.

For the description of mass transfer the penetration theory according to Higbie has been applied. The disadvantage of more

Table 1
Component reaction rates

| Component | Model ABP | Model BPdot | Model 3T |
|---|---|---|---|
| A | $R_A = -k_1 \cdot [A] \cdot [B]$ | $R_A = -R_2$ | $R_A = -R_2$ |
| B | $R_B = -k_1 \cdot [A] \cdot [B]$ | $R_B = -R_3$ | $R_B = -R_1 - R_3$ |
| P | $R_P = k_1 \cdot [A] \cdot [B]$ | $R_P = R_3$ | $R_P = R_3$ |
| In• | – | – | $R_{In\bullet} = -R_1$ |
| In | – | – | $R_{In} = R_1$ |
| $T_1$ | – | – | $R_{T1} = R_4$ |
| $T_2$ | – | – | $R_{T2} = R_5$ |
| $T_3$ | – | – | $R_{T3} = R_6$ |
| B• | – | $R_{B\bullet} = -R_2 + R_3$ | $R_{B\bullet} = R_1 - R_2 + R_3 - 2 \cdot R_4 - R_5$ |
| P• | – | $R_{P\bullet} = R_2 - R_3$ | $R_{P\bullet} = R_2 - R_3 - R_5 - 2 \cdot R_6$ |

complicated numerical calculations in the penetration theory in comparison to the film theory is compensated by more physically realistic descriptions (Versteeg et al., 1987). In the penetration theory the equation for a single diffusing and reacting component (i) is given by

$$\frac{\partial C_i}{\partial t} = D_i \cdot \frac{\partial^2 C_i}{\partial x^2} + R_i, \tag{10}$$

initial condition: $t = 0$ and $x \geqslant 0$, $C_i = C_{i,\text{bulk}}$, (11)

boundary conditions: $t > 0$ and $x = \infty$, $C_i = C_{i,\text{bulk}}$, (12)

$t > 0$ and $x = 0$ $J_{i,\text{gas}} = J_{i,\text{liquid}}$. (13)

In the application of the first boundary condition, Eq. (12), the bulk concentration of the absorbing species A is set to zero. This is allowed in the present study because only irreversible reactions are considered. The second boundary condition states that the flux of component $i$ in the gas phase is equal to the flux in the liquid phase. The expressions for the reaction rates differ for each model but all reaction rates are derived from the stoichiometry of the molecular reactions. For the BPdot and 3T model the rates for the reactions are defined as

$$\begin{aligned} R_1 &= k_1 \cdot [In\bullet] \cdot [B], \\ R_2 &= k_2 \cdot [A] \cdot [B\bullet], \\ R_3 &= k_3 \cdot [B] \cdot [P\bullet], \\ R_4 &= k_4 \cdot [B\bullet]^2, \\ R_5 &= k_5 \cdot [B\bullet] \cdot [P\bullet], \\ R_6 &= k_6 \cdot [P\bullet]^2. \end{aligned} \tag{14}$$

The overall component reaction rate expressions are given in Table 1. The concentration profiles and derived properties are evaluated at the end of the contact time, $\tau_p$. The contact time for absorption according to the penetration model is directly related to the liquid mass transfer coefficient and the diffusion coefficient of component A by means of

$$\tau_p = 4 \cdot \frac{D_A}{\pi \cdot k_L^2}. \tag{15}$$

To display the concentration profiles in a more convenient way a scaling factor is derived from the solution of the penetration model for a non-reacting diffusion system (Westerterp et al., 1990):

$$c_A(x,t) = c_{A,i} \cdot \left[1 - \text{erf}\left(\frac{x}{2\sqrt{D_A \cdot t}}\right)\right]. \tag{16}$$

At any time $t$, the value of $x$ for which the error function is close enough to unity to reduce the concentration of A to zero is not precisely determined. The error function of the square root of $\pi$ is close to 0.99 and this value is combined with $\tau_p$ to define the penetration depth, $\delta_p$:

$$\frac{\delta_p}{2\sqrt{D_A \cdot \tau_p}} = \sqrt{\pi}. \tag{17}$$

Substitution of Eq. (15) for $\tau_p$ gives

$$\delta_p = 4.\frac{D_A}{k_L}. \tag{18}$$

The choice for the square root of $\pi$ is arbitrary, but as any other value for $x$ would be equally disputable the esthetical result of Eq. (18) is preferred.

## 3. Numerical treatment

The system of coupled non-linear parabolic partial differential equations hasas been solved by application of a method presented by Cornelisse et al. (1980). This approach is based on a three-point backward scheme for finite differencing by Baker and Oliphant (1960). For an efficient use of grid point allocation, transformation of both the time and spatial variables has been applied (Versteeg et al., 1989). The transformation of the time variable is given by

$$t = \tau_p \cdot s^4, \tag{19}$$

where $\tau_p$ is the specific contact time defined by Eq. (8). The spatial grid is allocated through a transform function comprising a parameter $p$ (varied between 0 and 1) through which the curvature can be controlled.

$$x = p \cdot z + (1 - p) \cdot z^4. \tag{20}$$

For small values of $p$ the number of grid points per distance increases in the direction of the gas/liquid interface. The method for finite differencing requires all equations to be linear in the domain of interest. Besides the differential terms the reaction rates are non-linear and therefore need to be transformed. The linearization of the reaction rate terms is performed through a first-order Taylor expansion around the reference component concentrations that have been calculated in the previous time step. The reaction rate equation can be written in general terms as

$$R_j = k_j \cdot \prod_{p=1}^{\text{comp}} C_p^{\beta_{p,j}}. \tag{21}$$

The exponent $\beta_{p,j}$ is the reaction order of component $p$ in the $j$th reaction. The component rate equation is

$$\mathrm{R}_i = \sum_{j=1}^{\mathrm{reac}} \nu_{i,j} \cdot \mathrm{R}_j. \tag{22}$$

The stoichiometric coefficient $\nu_{i,j}$ indicates the coefficient of component $i$ in reaction $j$. The combination of Eqs. (21) and (22) in the linearization based on a Taylor expansion around $C_i^\circ$ gives

$$\mathrm{R}_i = \sum_{j=1}^{\mathrm{reac}} \nu_{i,j} \cdot k_j \cdot \left[1 - \sum_{p=1}^{\mathrm{comp}} \beta_{p,j}\right] \cdot \prod_{p=1}^{\mathrm{comp}} (C_p^\circ)^{\beta_{p,j}} + \sum_{p=1}^{\mathrm{comp}} \left\{ \sum_{j=1}^{\mathrm{reac}} \nu_{i,j} \cdot k_j \cdot \frac{\beta_{p,j}}{C_p^\circ} \cdot \prod_{q=1}^{\mathrm{comp}} (C_q^\circ)^{\beta_{q,j}} \cdot C_p \right\}. \tag{23}$$

Details of this derivation are given in the Appendix. The discretizations of the differentials are identical to the schemes applied by Cornelisse et al. (1980). The differentials in Eq. (10) are transformed to

$$\frac{\partial C_i}{\partial t} \to \frac{1}{f'(s)} \cdot \frac{3 \cdot C_{i,m}^{n+1} - 4 \cdot C_{i,m}^{n} + C_{i,m}^{n-1}}{2 \cdot \Delta s} \tag{24}$$

$$\frac{\partial^2 C_i}{\partial x^2} \to \left\{ \frac{1}{g'(z)^2} \cdot \frac{1}{\Delta z^2} - \frac{3}{2} \cdot \frac{g''(z)}{g'(z)^3} \cdot \frac{1}{\Delta z} \right\} \cdot C_{i,m-1}^{n+1} - 2 \cdot \left\{ \frac{1}{g'(z)^2} \cdot \frac{1}{\Delta z^2} - \frac{g''(z)}{g'(z)^3} \cdot \frac{1}{\Delta z} \right\} \cdot C_{i,m}^{n+1} + \left\{ \frac{1}{g'(z)^2} \cdot \frac{1}{\Delta z^2} - \frac{1}{2} \cdot \frac{g''(z)}{g'(z)^3} \cdot \frac{1}{\Delta z} \right\} \cdot C_{i,m-1}^{n+1}. \tag{25}$$

The derivatives of the transformation functions are given by

$$f'(s) = 4 \cdot \tau_p \cdot s^3, \tag{26}$$

$$g'(z) = p + 4 \cdot (1 - p) \cdot z^3, \tag{27}$$

$$g''(z) = 12 \cdot (1 - p) \cdot z^2. \tag{28}$$

The boundary condition at the gas/liquid interface, Eq. (13), is included as the flux condition in the transformed and discretized equation (Cornelisse et al., 1980).

$$-D_i \cdot \left.\frac{\partial C_i}{\partial x}\right|_{x=0} = k_G \cdot \left( C_{i,\mathrm{gas}} - \frac{C_{i,x=0}}{\mathrm{mgl}_i} \right). \tag{29}$$

Application of the transformation for $x$ and a number of straightforward rearrangements leads to

$$\left.\frac{\partial^2 C_i}{\partial x^2}\right|_{x=0} \to \frac{1}{g'(z)^2} \cdot \frac{2}{\Delta z^2} \cdot (C_{i,1}^{n+1} - C_{i,0}^{n+1}) + \left( \frac{1}{g'(z)} \cdot \frac{2}{\Delta z} + \frac{g''(z)}{g'(z)^2} \right) \cdot \frac{k_G}{D} \cdot \left( C_{i,\mathrm{gas}} - \frac{C_{i,g(z)=0}}{\mathrm{mgl}} \right). \tag{30}$$

The boundary conditions at $x = \infty$ are approximated by extending the grid to a depth in the liquid sufficiently larger than the penetration depth as defined by Eq. (18). Taking the range of the depth in the liquid as five times the penetration depth is assumed to be sufficient. This assumption has been checked on a number model calculations by inspection of the gradients. All checks revealed that the gradients were sufficiently close to zero at $x = 5\delta_p$.

In the first time step the three-point backward discretization is replaced by a two-point Euler discretization because before $t = 0$ no time step exists. Since the first time step is very small (due to the transformation of $t$), the larger truncation error of the Euler step is considered to be acceptable.

In all the models only component A is absorbed from the gas phase, therefore the calculation of enhancement factors is only concerned with component A and performed according to

$$E = \frac{\int_0^{\tau_P} -D_\mathrm{A} (\mathrm{d}C_\mathrm{A}/\mathrm{d}x)|_{x=0} \, \mathrm{d}t}{k_L \cdot \tau_P \cdot (C_\mathrm{A}|_{x=0} - C_{\mathrm{A,bulk}})}. \tag{31}$$

The gradient at $x = 0$ is calculated by means of Eq. (29). The integral from 0 to $\tau_P$ is approximated by the summation of the gradients over all time steps (integration by trapezium rule).

## 4. Model simulations

The number of parameters that can be varied in the models is too large to treat all in detail, therefore only the most interesting parameters have been selected. The emphasis has been set on reaction rate constants and diffusion coefficients in order to examine the influence of the reactive intermediates. Therefore, the gas phase concentrations and gas–liquid partition coefficients are kept constant as well as the liquid phase concentrations at $t = 0$ and in the liquid bulk. In addition, $k_G$ and $k_L$ were kept constant. For $k_G$ the value was chosen sufficiently high to eliminate gas film resistances (e.g. 100 m/s). The liquid side mass transfer coefficient $k_L$ has been fixed at $5 \times 10^{-5}$ m/s, a typical value for gas–liquid reactors. All components except A are considered to be non-volatile. In the models these components have been given (extremely) high solubility coefficients. In addition, the diffusion coefficients of these non-volatile components have no interaction with $k_L$ and can therefore be varied without affecting the contact time or penetration depth.

For all components, unless specified otherwise, the following default values have been applied: $C_{i,\mathrm{gas}} = 10^{-40}$ kmol/m$^3$, $C_i = 10^{-40}$ kmol/m$^3$, $D_i = 10^{-9}$ m$^2$/s and $\mathrm{mgl}_i = 10^{40}$. In all models the gas phase concentration for A is $C_{\mathrm{A,gas}} = 1$ kmol/m$^3$, the liquid bulk concentration for B is $C_\mathrm{B} = 2$ kmol/m$^3$ and the solubility coefficient for A is $\mathrm{mgl}_\mathrm{A} = 3$. The default concentration of B• is $10^{-5}$ kmol/m$^3$. The default values for the reaction rate constants are listed in Table 2.

The number of spatial grid points has been set to 800 for all simulations. The number of grid points for the time coordinates was standard set to 60. In cases where a higher precision in the calculated enhancement factors was desired, the number of grid points was increased to 600.

## 5. Position and shape of the reaction front

For fast reactions between A and B the region in the liquid where both A and B exist in significant concentrations is very small. For infinitely fast reactions this region coincides with a single point. This is the point (or region) where the reaction rate between A and B is maximum and is called reaction front. The diffusion coefficients of reactant B and intermediate B• influence the position and shape of the reaction front. For comparison the results of the reaction A + B → P are included. The analytical solutions have been calculated with Eqs. (3) and (4). The positions of the reaction fronts are given in Table 3. The positions are scaled with the penetration depth as defined by Eq. (18). For model ABP the differences between the analytical and numerical solutions are small (less than 0.5% for the cases studied). Both the analytical solution and the numerical results agree on the large shift in position of the reaction front by changing the diffusion coefficient of B. The shift of the position of the reaction front is illustrated in Fig. 2. In this figure the local reaction rates of the overall reaction A + B → P, based on the actual concentrations of the various species, are calculated from the concentration profiles emerging at the end of the contact time. For the analytical solution this results in a front that is a sharp single line, indicated by the dotted lines in Fig. 2. With a diffusion coefficient of B of $1 \times 10^{-9}\,m^2/s$ all models predict the position of the reaction front within close distance from each other. However, on a smaller scale of the penetration depth the profiles of the overall reaction rates of model BPdot and model 3T deviate as shown in Fig. 3. This behaviour is also observed with $D_c(B) = 1 \times 10^{-8}\,m^2/s$ (Fig. 4). Comparing Figs. 3 and 4, it is observed that the reaction rate profiles are more symmetrical when the diffusion coefficients of B and B• are equal. From Table 3 it appears that the location of the reaction rate maximum is equal to the analytical solution of theABP model when the diffusion coefficients of B and B• are equal. In case $D_c(B•)$ is not equal to $D_c(B)$ the model results differ from the analytical solution. With $D_c(B) = 1 \times 10^{-8}\,m^2/s$ these differences are more clear. Finally, from Table 3 it is observed that the BPdot model and the 3T model give identical solutions for the reaction front positions. If the diffusion coefficient of B differs from that of B• the shape of the reaction rate profile is non-symmetrical (Figs. 3b and 4a). For $D_c(B•) > D_c(B)$ as in Fig 3b the reaction profile is stretched (less steep) in the direction of the bulk of the liquid. The high diffusion rate of B• results in lower concentration of B• from the reaction front towards the bulk liquid. This causes a (small) increase in the concentration of A in the bulk direction (see Fig. 5). These observations are only valid for fast reactions as with slow to moderate fast reactions the reaction front is widely spread or not present at all.

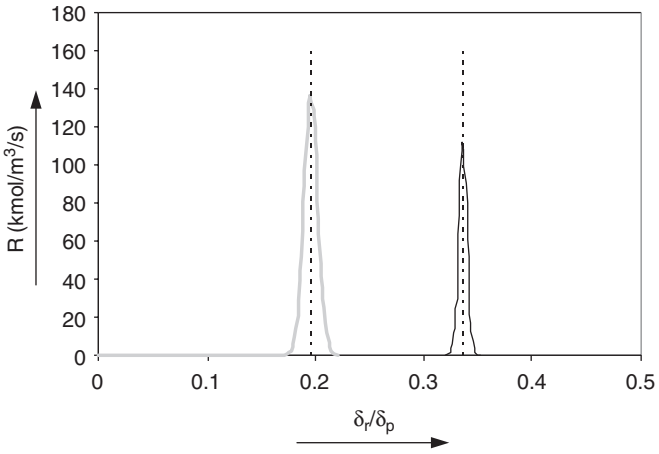


Fig. 2. Reaction rate as function of penetration depth for model ABP. Solid lines are numerical calculated results, dotted vertical lines are reaction front positions according to Eqs. (3) and (4). $D_c(B) = 1 \times 10^{-8}\,m^2/s$ (left peak) and $D_c(B) = 1 \times 10^{-9}\,m^2/s$ (right peak).

Table 2
Default second order reaction rate constants (in $kmol/m^3/s$) for model simulations

| Reaction | Model | | |
|---|---|---|---|
| | ABP | BPdot | 3T |
| A + B → P | $1 \times 10^6$ | | |
| A + B• → P• | | $1 \times 10^8$ | $1 \times 10^8$ |
| P• + B → P + B• | | $1 \times 10^9$ | $1 \times 10^9$ |
| 2B• → $T_1$ | | | $1 \times 10^5$ |
| B• + P• → $T_2$ | | | $1 \times 10^5$ |
| 2P• → $T_3$ | | | $1 \times 10^5$ |
| B + In• → B• + In | | | $1 \times 10^9$ |

Table 3
Reaction front positions

| Model | $D_c(B)$ $(m^2/s)$ | $D_c(B•)$ $(m^2/s)$ | $\delta_r/\delta_p$ Analytical | Numerical |
|---|---|---|---|---|
| ABP | $1 \times 10^{-9}$ | – | 0.336 | 0.335 |
| BPdot | $1 \times 10^{-9}$ | $1 \times 10^{-9}$ | | 0.335 |
| | $1 \times 10^{-9}$ | $1 \times 10^{-8}$ | | 0.333 |
| 3T | $1 \times 10^{-9}$ | $1 \times 10^{-9}$ | | 0.335 |
| | $1 \times 10^{-9}$ | $1 \times 10^{-8}$ | | 0.331 |
| ABP | $1 \times 10^{-8}$ | – | 0.194 | 0.196 |
| BPdot | $1 \times 10^{-8}$ | $1 \times 10^{-9}$ | | 0.202 |
| | $1 \times 10^{-8}$ | $1 \times 10^{-8}$ | | 0.196 |
| 3T | $1 \times 10^{-8}$ | $1 \times 10^{-9}$ | | 0.205 |
| | $1 \times 10^{-8}$ | $1 \times 10^{-8}$ | | 0.196 |

## 6. Influence of radical intermediates on the concentration profiles

The influence of the diffusion coefficient of B• on the concentration profiles near the gas–liquid interface has been examined for the 3T model. The occurrence of unequal diffusion coefficients for radicals with similar molecular weights is derived from the option of B• having an exchange reaction with B:

$$B + B• \rightleftharpoons B + B•. \tag{32}$$

The effective diffusion coefficient for B• can be higher by the exchange reaction (Ruff and Friedrich, 1971). In autoxidation

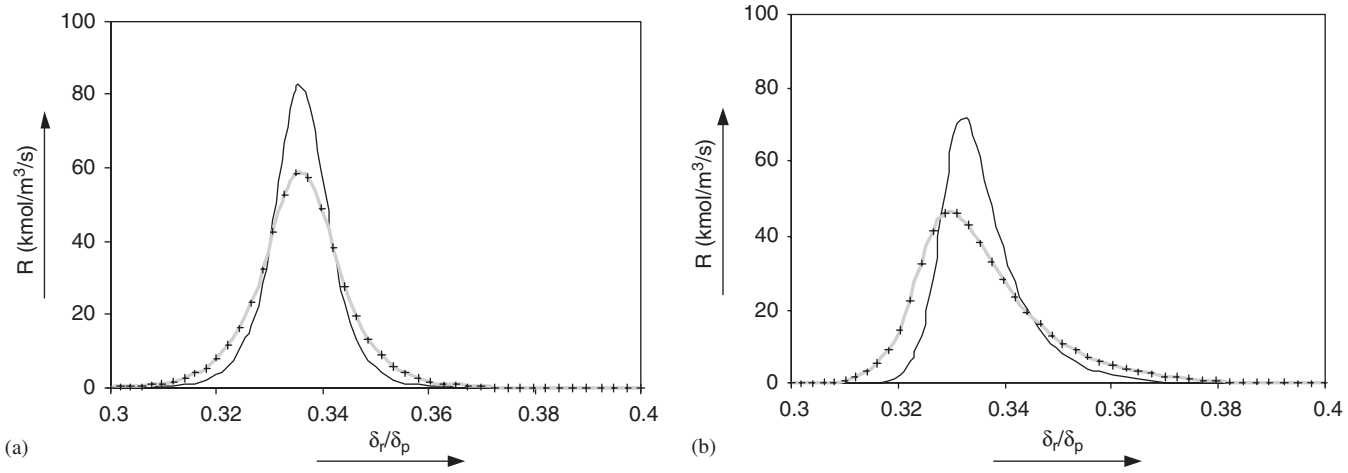


Fig. 3. Reaction rates in the liquid for $D_c(\mathrm{B}) = 1 \times 10^{-9}\,\mathrm{m}^2/\mathrm{s}$ at time $\tau_p$ for model BPdot (thin lines) and model 3T (grey lines and symbols): (a) $D_c(\mathrm{B}\bullet) = 1 \times 10^{-9}\,\mathrm{m}^2/\mathrm{s}$; (b) $D_c(\mathrm{B}\bullet) = 1 \times 10^{-8}\,\mathrm{m}^2/\mathrm{s}$.

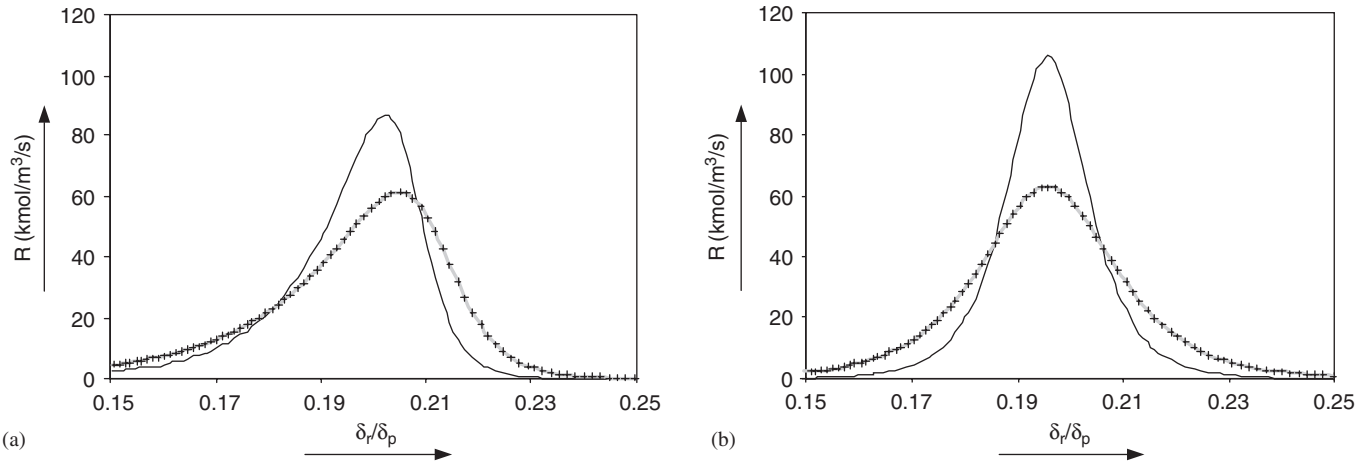


Fig. 4. Reaction rates in the liquid for $D_c(\mathrm{B}) = 1 \times 10^{-8}\,\mathrm{m}^2/\mathrm{s}$ at time $\tau_p$ for model BPdot (thin lines) and model 3T (grey lines and symbols): (a) $D_c(\mathrm{B}\bullet) = 1 \times 10^{-9}\,\mathrm{m}^2/\mathrm{s}$; (b) $D_c(\mathrm{B}\bullet) = 1 \times 10^{-8}\,\mathrm{m}^2/\mathrm{s}$.

reactions radical types corresponding to the solvent are well known, i.e., the benzyl radical in oxidation of toluene and the cyclohexyl radical in the oxidation of cyclohexane. The results for the simulations are presented in the form of concentration profiles at the end of the contact time.

The B• and P• concentration profiles for varying $D_c(\mathrm{B}\bullet)$ are shown in Figs. 6 and 7, respectively. The concentrations for the radical intermediates are scaled to the total concentration of radicals at $t = 0$. In Fig. 6 the concentration profiles for B• appear to have two distinct regions: Firstly where the concentration has been lowered by pure diffusion of B• to the reaction zone ($x/\delta_{\mathrm{film}} > 0.4$). Secondly, a region near the reaction zone where the concentration of B• has been decreased much more rapidly as a result of reaction ($x/\delta_{\mathrm{film}}$ between 0.3 and 0.35). For P• (Fig. 7) a similar behaviour is observed; however, the effect of a higher diffusion coefficient for B• is opposite to that observed for the B• concentration: the concentration of P• builds up as $D_c(\mathrm{B}\bullet)$ is increased. The concentration of

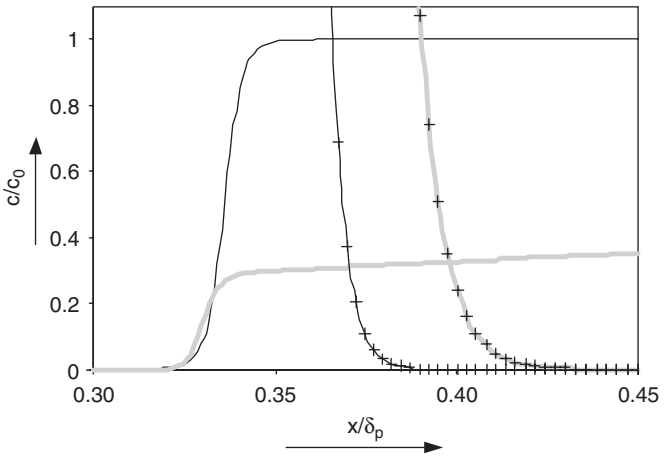


Fig. 5. Model BPdot: concentrations of B• (lines) and A (lines and symbols) for $D_c(\mathrm{B}\bullet) = 1 \times 10^{-9}\,\mathrm{m}^2/\mathrm{s}$ (thin black lines), $D_c(\mathrm{B}\bullet) = 1 \times 10^{-8}\,\mathrm{m}^2/\mathrm{s}$ (wide grey lines). Scale factor $c_0$ is the total concentration of radicals at $t = 0$.

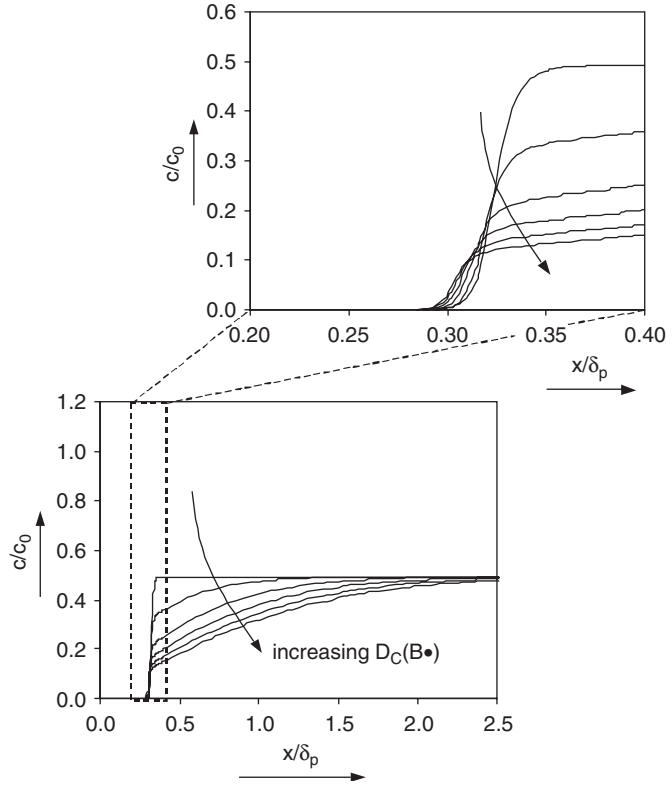


Fig. 6. Concentration profiles of B• for model 3T. $D_c$(B•) is varied between $1 \times 10^{-9}$ m$^2$/s to $1 \times 10^{8}$ m$^2$/s.

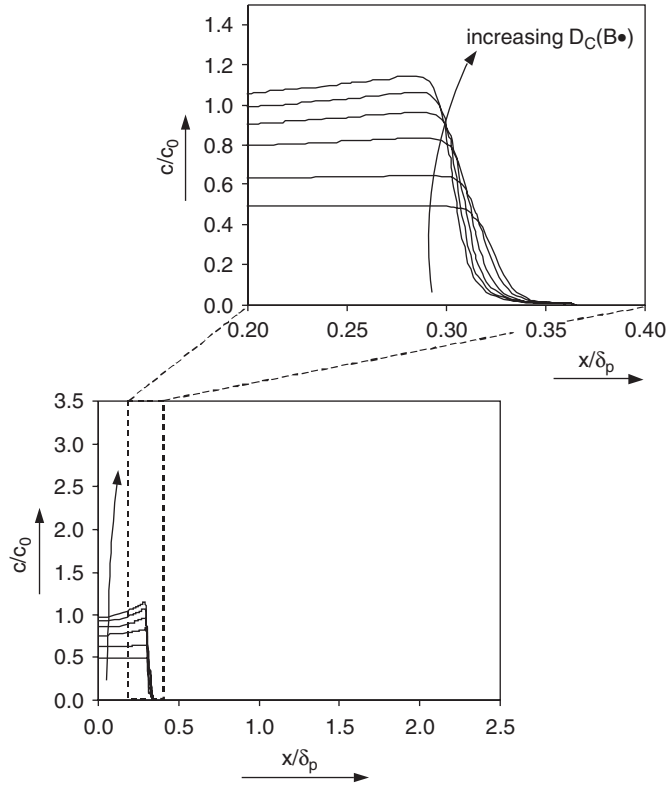


Fig. 7. Concentration profiles of P• for model 3T. $D_c$(B•) is varied between $1 \times 10^{-9}$ m$^2$/s to $1 \times 10^{8}$ m$^2$/s.

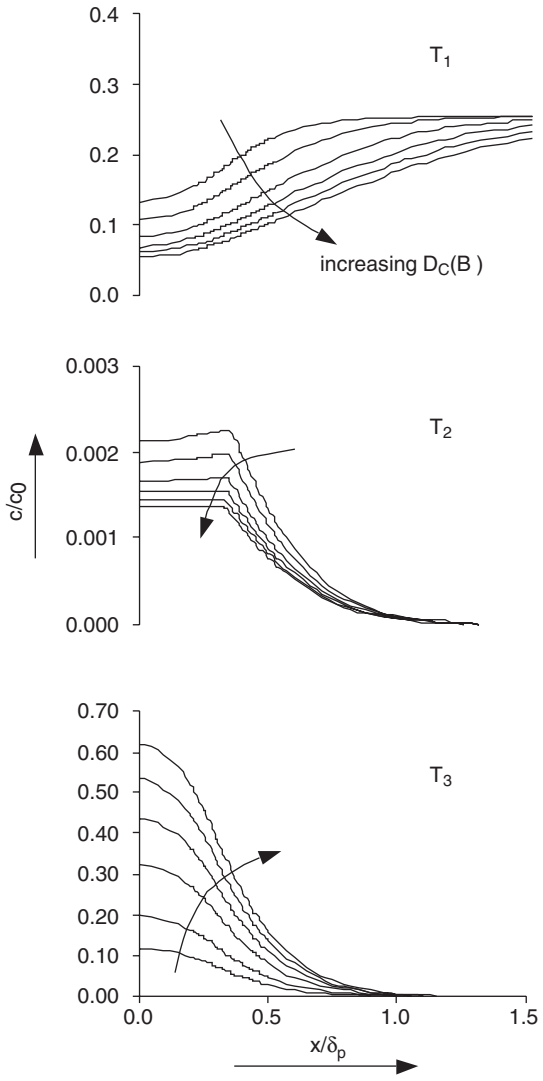


Fig. 8. Concentration profiles of termination products $T_1$, $T_2$ and $T_3$ for model 3T. $D_c$(B•) is varied between $1 \times 10^{-9}$ m$^2$/s and $1 \times 10^{-8}$ m$^2$/s.

P• has a maximum located quite close to the reaction zone. Between the G/L interface and the reaction front the concentration of B is zero, any P• formed cannot react with B• hence all radicals are present as P•. The termination reaction between P• radicals reduces the concentration near the interface. The consumption of P• is compensated via diffusion from the reaction zone where P• is product. For higher values of $D_c$(B•) the production of P• is increased leading to higher concentrations of P• near the reaction zone relative to the gas–liquid interface.

The profiles of B• and P• are reflected in the termination products. For equal reaction rate constants the ratio between the symmetrical termination products ($T_1$ and $T_3$) varies depending on the relative diffusion coefficients of the radical intermediates, see Fig. 8. The mixed termination product $T_2$ has in all cases the lowest concentrations because the regions where both B• and P• are present in non-zero quantities are very limited.

## 7. Design aspects

One of the key parameters for the design of a gas–liquid reaction system is the absorption rate of the gaseous component. Estimation of this rate from other (known) parameters is often very much desired. To quantify the absorption rates, the effect of a number of variables on calculated enhancement factors is demonstrated for the models described in this paper. The different number of parameters applied in each model require additional consideration, however. For the translation of complex models to simple models and vice versa functions are required that correlate the parameters of the different model versions. The form of the function and the inclusion of additional parameters determine the quality of the results of the simplified model in comparison to the complex model as well as the effort that has to be delivered to obtain the simplified model results. One example is the dependency of $E$ on reaction rate constants in the models BPdot and 3T, respectively, versus model ABP; whereas model ABP only has a single rate constant, the model BPdot has two reactions and model 3T has six reactions. The next section is focussed on model BPdot to demonstrate some basic features without the complications involved with handling the multiple reactions of model 3T. The enhancement factor (calculated according to Eq. (31)) as function of the Hatta number ($\varphi$) is a simple plot for model ABP as shown in Fig. 9. The definition for Hatta for this type of reaction is

$$\varphi = \frac{\sqrt{k_1 \cdot c_B \cdot D_A}}{k_L}, \tag{33}$$

The kinetic rate constant $k_1$ is related to model ABP (not to be confused with the $k_1$ from model 3T, Eq. (7)). For models comprising more than one reaction of the gaseous reactant, the definition of the Hatta number is not straightforward because in more complex reaction schemes reactant A can be consumed in various ways, e.g., parallel, consecutive and combinations of these paths. For the case of the BPdot model, two parameters are proposed based on the Hatta number of a single reaction:

$$\varphi_2 = \frac{\sqrt{k_2 \cdot c_{dot} \cdot c_B \cdot D_A}}{k_L}, \tag{34}$$

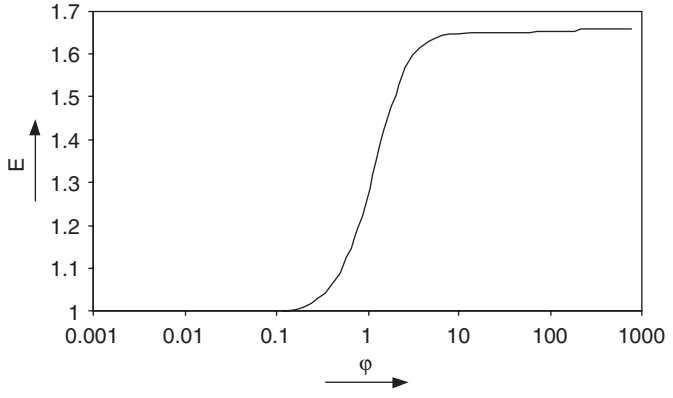


Fig. 9. Enhancement factor as function of the Hatta number for model ABP, $E = 1.657$ for high values of Hatta.

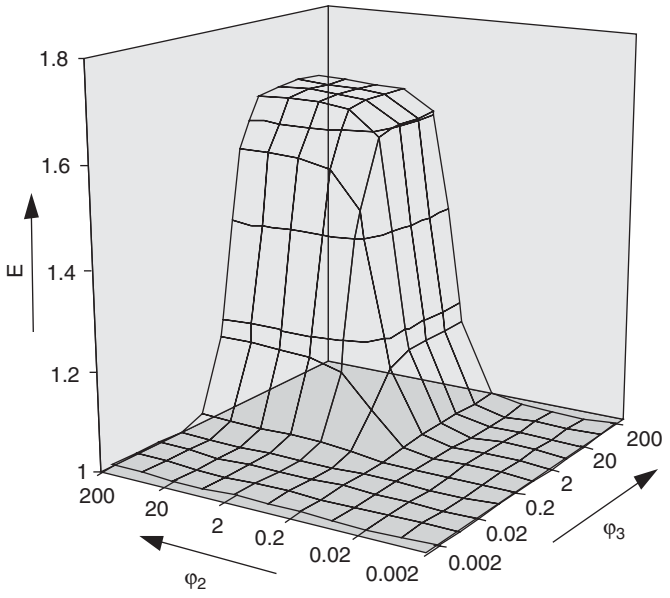


Fig. 10. Enhancement factor as function of the parameters $\varphi_2$ and $\varphi_3$ of model BPdot, $E = 1.656$ for high values of $\varphi_2$ and $\varphi_3$.

$$\varphi_3 = \frac{\sqrt{k_3 \cdot c_{dot} \cdot c_B \cdot D_A}}{k_L}. \tag{35}$$

The concentration $c_{dot}$ is the concentration of initiator (In•) at $t = 0$. It is easily verified that

$$\varphi = \sqrt{\varphi_2^2 + \varphi_3^2} \quad \text{or} \quad k_1 = (k_2 + k_3) \cdot c_{dot}. \tag{36}$$

The 3D-representation of the enhancement factor calculated with model BPdot is shown in Fig. 10.

To transform the enhancement factor for the single reaction ABP model to a representation similar to that of Fig. 10, it is assumed that the single reaction is also composed of two contributions. These two contributions are not determined by a physical or chemical process but purely by a mathematical relation. One example of such a mathematical function is Eq. (36). Any combination of $\varphi_2$ and $\varphi_3$ gives a Hatta number $\varphi$ in the ABP model. The enhancement factor for the ABP model is calculated from $\varphi$ . The enhancement factor as function of $\varphi_2$ and $\varphi_3$ is shown in Fig. 11. From the comparison of Figs. 10 and 11 it is clear that only for a limited number of combinations of $\varphi_2$ and $\varphi_3$ the enhancement factor of the BPdot model coincides with the factor calculated for the ABP model. The relative differences between model ABP and BPdot are shown in Fig. 12. The deviation of model ABP compared to model BPdot is scaled by the enhancement factor at infinitely high reaction ($E_{A,\infty}$) according to

$$\Delta(E) = \frac{E_{(ABP)} - E_{(BPdot)}}{E_{A,\infty} - 1}. \tag{37}$$

The graph in Fig. 12 is slightly rotated compared to the previous two figures to show the area for high $\varphi_2$ and $\varphi_3$ values more clearly. For the design of a reactor system the areas where the use of the simplified model leads to good approximations can be easily identified from Fig. 12. The symmetry in

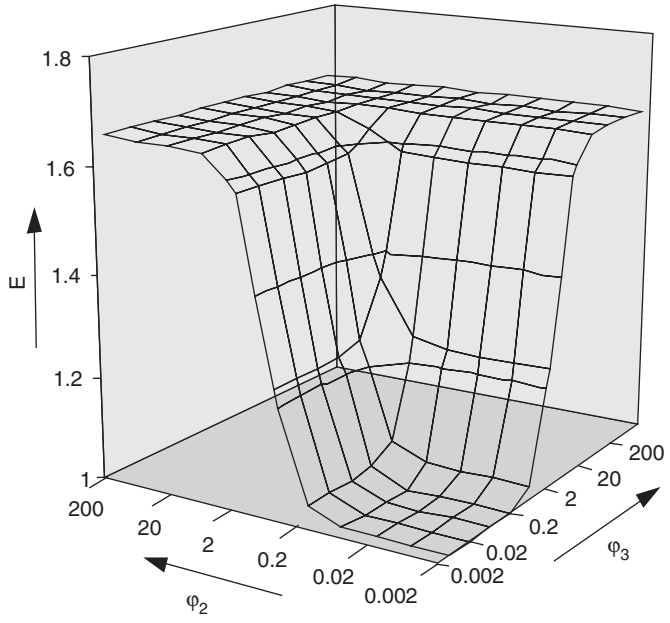


Fig. 11. Enhancement factor for model ABP as function of the parameters $\varphi_2$ and $\varphi_3$.

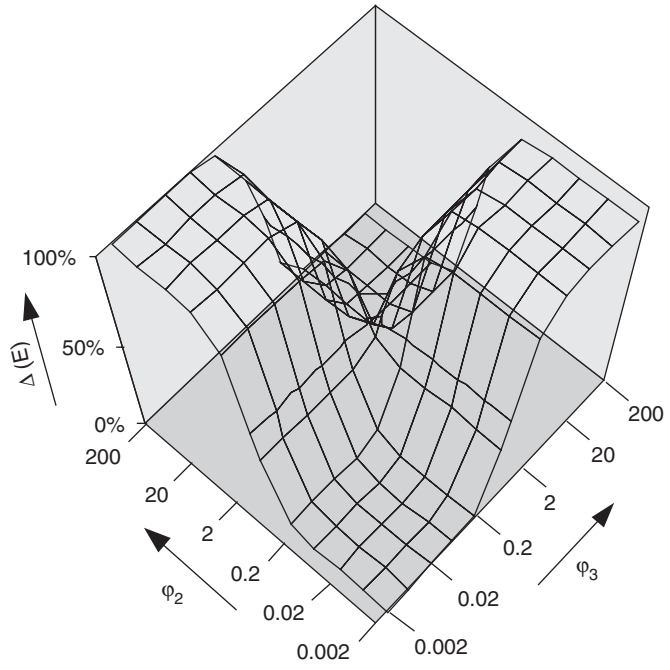


Fig. 12. Deviation of enhancement factors as calculated by model ABP compared to model BPdot as function of the parameters $\varphi_2$ and $\varphi_3$.

Fig. 12 suggests that as long as the reaction rates of the radical intermediates are more or less balanced the approximation of a reaction without intermediates is valid regardless of the value of the enhancement factor. In the areas where the values of $\varphi_2$ and $\varphi_3$ differ significantly the radicals in model BPdot exist effectively only in one kind, B• or P•, depending on which of the two parameters is larger. In this way the reaction

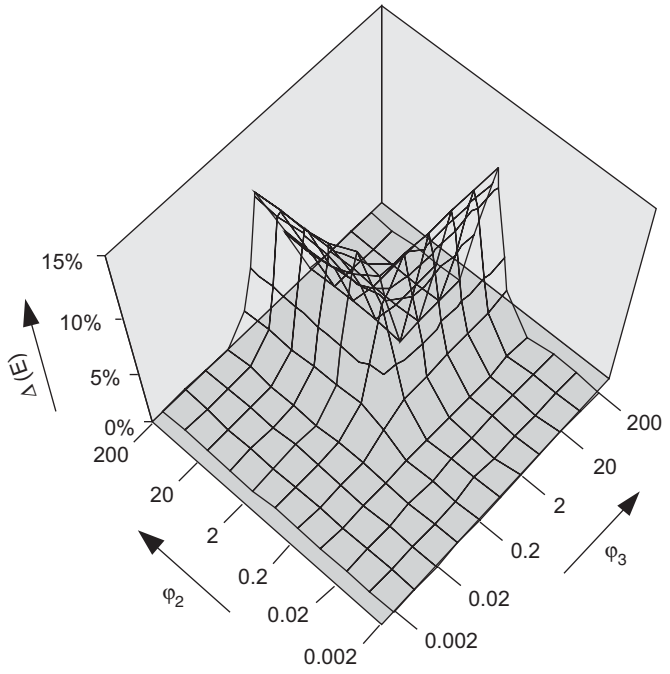


Fig. 13. Deviation of enhancement factors as calculated by model ABP with transfer by Eq. (38) compared to model BPdot as function of the parameters $\varphi_2$ and $\varphi_3$.

path is blocked and no enhancement of mass transfer occurs, e.g. $E=1$. The correlation for the translation to the ABP model, Eq. (36), assigns a value for $k_1$ that is still quite large and therefore an enhancement factor bigger than 1 is derived.

The form of Eq. (36) suggests that the overall reaction rate is determined by the sum of the two (radical) reactions. By adding a weight on the summation of $k_2$ and $k_3$, it is possible to account for the effect of large differences in values for $\varphi_2$ and $\varphi_3$. One example is the function:

$$k_1 = \frac{k_2 \cdot k_3}{k_2 + k_3} \cdot c_{\mathrm{dot}}. \tag{38}$$

This correlation does not introduce additional parameters but for unequal values of $k_2$ and $k_3$ (or $\varphi_2$ and $\varphi_3$) the value of $k_1$ is determined by the smallest value of $k_2$ or $k_3$. In physical terms: the overall rate is determined by the slowest step. The result for transformation according to Eq. (38) resembles the enhancement factors of model BPdot (Fig. 10) much closer than in case of the application of Eq. (36). The differences between the model ABP with the transformation according to Eq. (38) and model BPdot is shown in Fig. 13. Comparing Figs. 12 and 13 it is clear that by the translation through Eq. (38) a better match between model ABP and model BPdot is obtained. In addition, the software code for model ABP does not have to be changed upon application of Eq. (38).

Functions other than Eq. (36) or (38) could be evaluated. When the BPdot model is simplified through a Bodenstein approximation (Helfferich, 2001a) the resulting expression is physically determined. The derivation of the equation is given

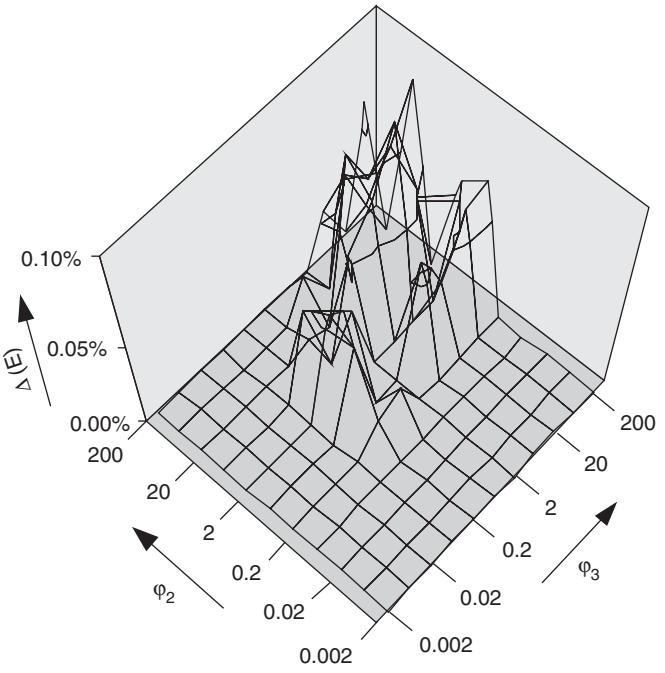


Fig. 14. Deviation of enhancement factors as calculated by model ABP with transfer by Eq. (39) compared to model BPdot as function of the parameters $\varphi_2$ and $\varphi_3$.

in Appendix B; the resulting transfer equation is

$$k_1 = \frac{k_2 \cdot k_3 \cdot c_{\mathrm{dot}}}{k_2 \cdot c_{\mathrm{A}} + k_3 \cdot c_{\mathrm{B}}}. \tag{39}$$

In contrast to Eqs. (36) and (38) this function contains the concentrations for A and B meaning that these concentrations need to be included in the calculations. An adaptation in the model ABP is required as the linearization of the reaction term, Eq. (23), is not valid for fractional reaction rate expressions as in Eq. (39). Instead of the generic expression for power laws presented in Appendix A, the analytical derivatives of Eq. (39) can easily be applied. These derivatives are also included in Appendix B. The results for model ABP transformed by application of Eq. (39) are nearly identical to the exact solution (calculated with model BPdot), see Fig. 14. The small scatter in the graph is mainly caused by the numerical precision because by reducing the precision this scatter is significantly increased (increasing the precision requires exponentially more computing time; the simulations for Fig. 14 required appr. 12 h with a 3 GHz processor).

A simplified model should meet the requirements for a specific job like for example incorporation in a CFD application or for the purpose of a process control study. Assuming that a complex model (derived from fundamental principles) is available and the requirements for the simplified model are known, it is possible to assign a very simple model as basic version. Then, by application of a number of transfer functions, alternatives of the basic version can be evaluated very easily.

Whether the availability of a complex model is essential for the proposed procedure is not clear yet. When the complex model can be replaced by for example discrete observations from experiments, this procedure can also be a recipe to determine a suitable simple model directly from experimental observations.

The study of the models ABP and BPdot is of course a very simplified exercise compared to most of the radical reaction networks known from literature. The complexity of the analysis rapidly increases with the number of components, but as long as the translation of process parameters in the complex reaction system towards simplified models can be performed by means of comparing observable responses, for example enhancement factors, it is possible to obtain a validated, fit-for-purpose simplified model.

Model 3T has been left out of the analysis of this section because the complexity of this model is not increased in terms of the intermediates or reaction pathways. Instead, the number of non-radical by-products is increased which requires the ABP model to be extended with reactions leading to those by-products. This would give an example where both the complex and simple models contain more variables, increased number of parameters and possible combinations, but the principles of the transfer functions are quite similar to the exercise with the BPdot and ABP models.

## 8. Conclusions

The calculation of enhancement factors applied in the design of a G/L reaction system can be performed with simplified models where the reactive intermediates do not occur in the expressions for the reaction rates. The optimum model for a specific design purpose can be found by tuning the function that correlates the parameters of the complex model to the reduced number of parameters of the simplified model. Depending on the choice of the form of the transfer function a large number of alternatives can be evaluated very easily. With transfer functions involving not only parameters but also process variables more effort in adaptations of the software routines in the model is required, but the agreement with the exact solution can be significantly improved.

The diffusion coefficients of radical intermediates have significant influence on the profiles of concentrations and reaction rates near the G/L interface. For fast reactions, all reactions take place in a small region. Increasing the diffusion coefficient of solvent radical (B•) reduces the concentration of B• near the reaction front. In the region between the G/L interface and the reaction front the concentration of the product radical (P•) builds up to higher values than the initial radical concentration at the start.

It is shown that for very fast reactions differences in diffusion coefficients of the intermediates can cause shifts in the by-product formation in other ways than often assumed (Helfferich, 2001b). The example for model 3T shows that the mixed termination product ($T_2$) from two radical intermediates B• and P• is only formed in low quantities because the two radicals do not occur in high concentrations simultaneously.

The numerical study of reaction mechanisms comprising reactive intermediates and fast reactions is very helpful in gaining

insight in effects that are difficult to study experimentally. This study has shown that systems with radical intermediates can be simplified to models where the intermediates are omitted. There is no reason that this methodology should be restricted to radical reactions. The extension to other systems as well the application on more complex systems than presented in this study is subject for future evaluations.

## Notation

| | |
|---|---|
| $a, b$ | stoichiometric coefficients |
| $c_{\text{dot}}, c_0$ | concentration radical species at $t = 0$, kmol/m$^3$ |
| $C$ | concentration, kmol/m$^3$ |
| $D, D_c$ | diffusion coefficient, m$^2$/s |
| $E$ | enhancement factor |
| $E_\infty$ | enhancement factor at infinitely fast reaction |
| $f, g$ | transformation functions |
| $J$ | flow across gas–liquid interface, kmol/m$^2$/s |
| $k$ | reaction rate constant, m$^3$/kmol/s |
| $k_G$ | gas side mass transfer coefficient, m/s |
| $k_L$ | liquid side mass transfer coefficient, m/s |
| mgl | solubility coefficient defined as $c_{\text{liquid}}/c_{\text{gas}}$ |
| $p$ | constant for curvature in $x$-variable transform function |
| $R$ | reaction rate, kmol/m$^3$/s |
| $s$ | transformed time variable |
| $t$ | time variable, s |
| $x$ | distance variable, m |
| $z$ | transformed distance variable |

*Greek letters*

| | |
|---|---|
| $\beta$ | constant defined in Eq. (1), m/s$^{0.5}$ |
| $\beta_{i,j}$ | exponent in the reaction rate equation of component $i$ in reaction $j$ |
| $\delta_p$ | penetration depth, m |
| $\delta_r$ | location of maximum reaction rate, m |
| $v_{i,j}$ | stoichiometric constant for component $i$ in reaction $j$ |
| $\tau_p$ | contact time, $s$ |
| $\varphi$ | Hatta number |
| $\varphi_2, \varphi_3$ | constants derived from $\varphi$ |

*Indices*

| | |
|---|---|
| $\circ$ | reference |
| bulk | liquid bulk |
| gas, liquid | phase |
| $i$ | any component |
| $j$ | any reaction |
| $n$ | time count finite difference equations |
| $m$ | distance count finite difference equations |
| $p, q$ | any component or reaction |

*Components*

| | |
|---|---|
| A | gas phase reactant |
| B | liquid phase reactant |
| B• | radical derived from B |
| In | deactivated radical initiator |
| In• | radical initiator |
| P | liquid phase product |
| P• | radical derived from P |
| $T_1$ | termination product formed out of reaction between two B• |
| $T_2$ | termination product formed out of reaction between B• and P• |
| $T_3$ | termination product formed out of reaction between two P• |

## Appendix A. Linearization of the reaction term by a Taylor series expansion around $C_i^\bullet$

In these equations the subscript $j$ is for the reaction indices and subscript $i$ is for components, they are replaced by $p$ and $q$ where appropriate.

Linearization of Eq. (21):

$$\mathrm{R}_j \to k_j \cdot \prod_{p=1}^{\text{comp}} (C_p^\bullet)^{\beta_{p,j}} + \sum_{p=1}^{\text{comp}} \left.\frac{\partial \mathrm{R}_j}{\partial C_p}\right|_\bullet \cdot (C_p - C_p^\bullet),$$

$$\left.\frac{\partial \mathrm{R}_j}{\partial C_p}\right|_\bullet = k_j \cdot \prod_{q=1, q\neq p}^{\text{comp}} (C_q^\bullet)^{\beta_{q,j}} \cdot \beta_{p,j} \cdot \frac{(C_p^\bullet)^{\beta_{p,j}}}{C_p^\bullet}. \tag{A.1}$$

Substituted in Eq. (22):

$$R_i = \sum_{j=1}^{\text{reac}} v_{i,j} \cdot k_j \cdot \left[ \prod_{p=1}^{\text{comp}} (C_p^\bullet)^{\beta_{p,j}} + \sum_{p=1}^{\text{comp}} \left\{ \prod_{q=1, q\neq p}^{\text{comp}} (C_q^\bullet)^{\beta_{q,j}} \cdot \beta_{p,j} \cdot \frac{(C_p^\bullet)^{\beta_{p,j}}}{C_p^\bullet} \cdot (C_p - C_p^\bullet) \right\} \right]. \tag{A.2}$$

Defining and simplification of the constant R-terms:

$$\mathrm{R}_i^{\text{const}} = \sum_{j=1}^{\text{reac}} v_{i,j} \cdot k_j \cdot \left[ \prod_{p=1}^{\text{comp}} (C_p^\bullet)^{\beta_{p,j}} - \sum_{p=1}^{\text{comp}} \left\{ \beta_{p,j} \cdot \prod_{q=1}^{\text{comp}} (C_q^\bullet)^{\beta_{q,j}} \right\} \right], \tag{A.3}$$

$$\mathrm{R}_i^{\text{const}} = \sum_{j=1}^{\text{reac}} v_{i,j} \cdot k_j \cdot \left[ 1 - \sum_{p=1}^{\text{comp}} \beta_{p,j} \right] \cdot \prod_{p=1}^{\text{comp}} (C_p^\bullet)^{\beta_{p,j}}. \tag{A.4}$$

Terms of R dependent on concentrations:

$$R_i^{Cp} = \sum_{j=1}^{reac} \nu_{i,j} \cdot k_j \cdot \sum_{p=1}^{comp} \left\{ \prod_{q=1,q\neq p}^{comp} (C_q^\bullet)^{\beta_{q,j}} \cdot \beta_{p,j} \cdot \frac{(C_p^\bullet)^{\beta_{p,j}}}{C_p^\bullet} \cdot C_p \right\}, \quad (A.5)$$

$$R_i^{Cp} = \sum_{p=1}^{comp} R_i(p), \quad (A.6)$$

$$R_i(p) = \sum_{j=1}^{reac} \nu_{i,j} \cdot k_j \cdot \beta_{p,j} \cdot (C_p^\bullet)^{\beta_{p,j}-1} \cdot \prod_{q=1,q\neq p}^{comp} (C_q^\bullet)^{\beta_{q,j}} \cdot C_p. \quad (A.7)$$

Eqs. (A.4) and (A.5) substituted in Eq. (A.2):

$$R_i = \sum_{j=1}^{reac} \nu_{i,j} \cdot k_j \cdot \left[ 1 - \sum_{p=1}^{comp} \beta_{p,j} \right] \cdot \prod_{p=1}^{comp} (C_p^\bullet)^{\beta_{p,j}} + \sum_{p=1}^{comp} \left\{ \sum_{j=1}^{reac} \nu_{i,j} \cdot k_j \cdot \frac{\beta_{p,j}}{C_p^\bullet} \cdot \prod_{q=1}^{comp} (C_q^\bullet)^{\beta_{q,j}} \cdot C_p \right\}. \quad (A.8)$$

## Appendix B. Bodenstein approximation for model BPdot

**Assumption 1.** The rate of formation and disappearance of B• are approximately equal:

$$R_1 = R_2,$$

$$k_2 \cdot c_A \cdot c_{B\bullet} = k_3 \cdot c_B \cdot c_{P\bullet}. \quad (B.1)$$

**Assumption 2.** The total radical concentration is constant and equal to the initial initiator concentration:

$$c_{B\bullet} + c_{P\bullet} = c_{dot}. \quad (B.2)$$

Rearrangement of Eq. (B.1) and substituted in Eq. (B.2):

$$c_{B\bullet} = \frac{c_{\bullet tot}}{1 + (k_2 \cdot c_A / k_3 \cdot c_B)}. \quad (B.3)$$

Eq. (B.3) is substituted in the expression for $R_1$:

$$R_1 = \frac{k_2 \cdot k_3 \cdot c_{dot}}{k_2 \cdot c_A + k_3 \cdot c_B} \cdot c_A \cdot c_B \quad (B.4)$$

The corresponding expression for model ABP is

$$R_1 = k_1 \cdot c_A \cdot c_B. \quad (B.5)$$

Reaction rates for the components are

$$R_i = \nu_i \cdot R_1,$$
$$\nu_i = -1 \quad \text{for } i = A \text{ or } B,$$
$$\nu_i = 1 \quad \text{for } i = P, \quad (B.6)$$

The partial derivatives are defined by

$$\frac{\partial R_i}{\partial c_A} = \nu_i \cdot \frac{k_2 \cdot k_3 \cdot c_{dot} \cdot c_B \cdot (k_2 \cdot c_A + k_3 \cdot c_B) - k_2^2 \cdot k_3 \cdot c_{dot} \cdot c_A \cdot c_B}{(k_2 \cdot c_A + k_3 \cdot c_B)^2}, \quad (B.7)$$

$$\frac{\partial R_i}{\partial c_B} = \nu_i \cdot \frac{k_2 \cdot k_3 \cdot c_{dot} \cdot c_A \cdot (k_2 \cdot c_A + k_3 \cdot c_B) - k_2 \cdot k_3^2 \cdot c_{dot} \cdot c_A \cdot c_B}{(k_2 \cdot c_A + k_3 \cdot c_B)^2}, \quad (B.8)$$

$$\frac{\partial R_i}{\partial c_P} = 0. \quad (B.9)$$

## References


Baker, G.A., Oliphant, T.A., 1960. An implicit, numerical method for solving the two-dimensional heat equation. Quarterly of Applied Mathematics 17, 361–373.

Burns, W.G., Hopper, M.J., Reed, C.R.V., 1970. Effects of L.E.T. and temperature in the radiolysis of cyclohexane. Part 2. Diffusion kinetic models. Transactions of the Faraday Society 66, 2182–2191.

Carey, F.A., Sundberg, R.J., 1990. Advanced Organic Chemistry, Part A: Structure and Mechanisms. Plenum Press, New York. pp. 676–677.

Cornelisse, R., Beenackers, A.A.C.M., Van Beckum, F.P.H., Van Swaaij, W.P.M., 1980. Numerical calculation of simultaneous mass transfer of two gases accompanied by complex reversible reactions. Chemical Engineering Science 35, 1245–1260.

Flores-Fernandez, G., Mann, R., 1978. Gas absorption with radical multiplying chain-type reactions. Chemical Engineering Science 33, 1545–1549.

Froment, G.F., Bischoff, K.B., 1990. Chemical Reactor Analysis and Design. Wiley, New York. pp. 275–282.

Helfferich, F.G., 2001a. Kinetics of homogeneous multistep reactions. In: Compton, R.G., Hancock, G. (Eds.), Comprehensive Chemical Kinetics, vol. 38. Elsevier, Amsterdam, pp. 72–77.

Helfferich, F.G., 2001b. Kinetics of homogeneous multistep reactions. In: Compton, R.G., Hancock, G. (Eds.), Comprehensive Chemical Kinetics, vol. 38. Elsevier, Amsterdam, pp. 283–286.

Juvekar, V.A., 1976. Gas absorption with autocatalytic reaction. Chemical Engineering Science 31, 91–92.

Ruff, I., Friedrich, V.J., 1971. Transfer diffusion. IV. A numerical test of the correlation between prototrope mobility and proton exchange rate of H3O+ and OH− ions with water. Journal of Physical Chemistry 75, 3297–3302.

Sim, M.-T., Mann, R., 1975. Gas absorption with autocatalytic reaction. Chemical Engineering Science 30, 1215–1218.

Sitarski, M., 1981. Effect of Brownian diffusion on chemical kinetics. International Journal of Chemical Kinetics 13, 125–133.

Van Swaaij, W.P.M., Versteeg, G.F., 1992. Mass transfer accompanied with complex reversible chemical reactions in gas–liquid systems: an overview. Chemical Engineering Science 47, 3181–3195.

Versteeg, G.F., Blauwhoff, P.M.M., Van Swaaij, W.P.M., 1987. The effect of diffusivity on gas–liquid mass transfer in stirred vessels. Experiments at atmospheric and elevated pressures. Chemical Engineering Science 42, 1103–1119.

Versteeg, G.F., Kuipers, J.A.M., Van Beckum, F.P.H., Van Swaaij, W.P.M., 1989. Mass transfer with complex reversible chemical reactions—I. Single reversible chemical reaction. Chemical Engineering Science 44, 2295–2310.

Westerterp, K.R., Van Swaaij, W.P.M., Beenackers, A.A.C.M., 1990. Chemical Reactor Design and Operation. Wiley, New York. pp. 357–494.